Non-Uniform Membrane Diffusion Enables Steady-State Cell Polarization via Vesicular Trafficking

Slaughter et al.

Supplementary Information

Supplementary Figure S1.

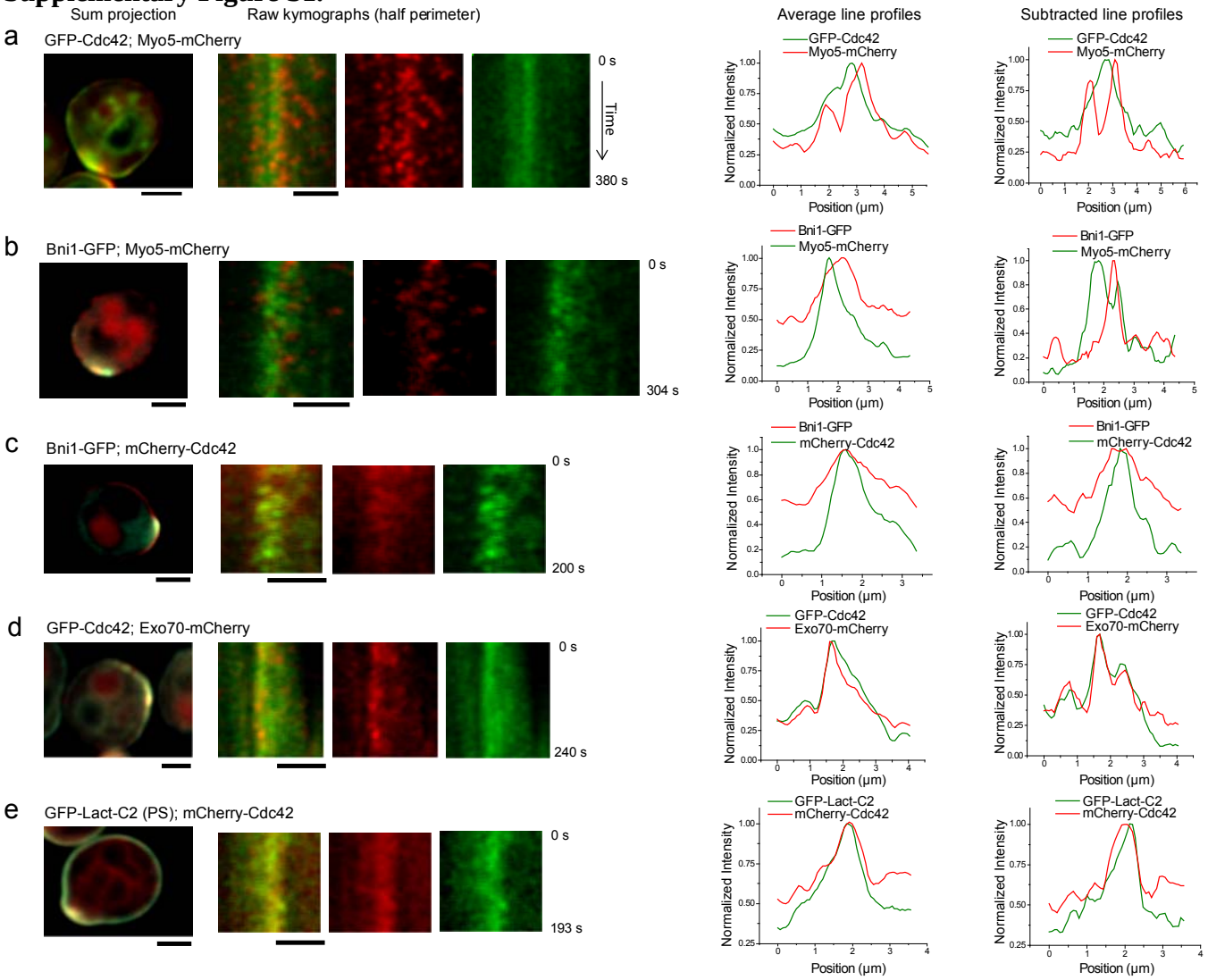

Supplementary Figure S1. Non-average subtracted data corresponding to the data shown in Figure 1. A time series-sum projection (left), along with raw kymographs (merged followed by individual channels) of GFP-Cdc42 with Myo5-mCherry (**a**), Bni1-GFP with Myo5-mCherry (**b**), Bni1-GFP with mCherry-Cdc42 (**c**), GFP-Cdc42 with Exo70-mCherry (**d**), and mCherry-Cdc42 with GFP-Lact-C2 (**e**). Scale bars: 2 μm. The plots on the right compare show normalized average line profiles (averaged over time for each kymograph) and a normalized average-subtracted single line profile for the green and red-labeled proteins. Note that on a cell perimeter-wide, average scale, there will be overlap of any pair of polarized proteins. However, line profiles generated from single images (without average subtraction (right column), or with average subtraction, show non-smooth distributions. (See also Figure 1 and Methods in Supplementary Information).

Supplementary Figure S2.

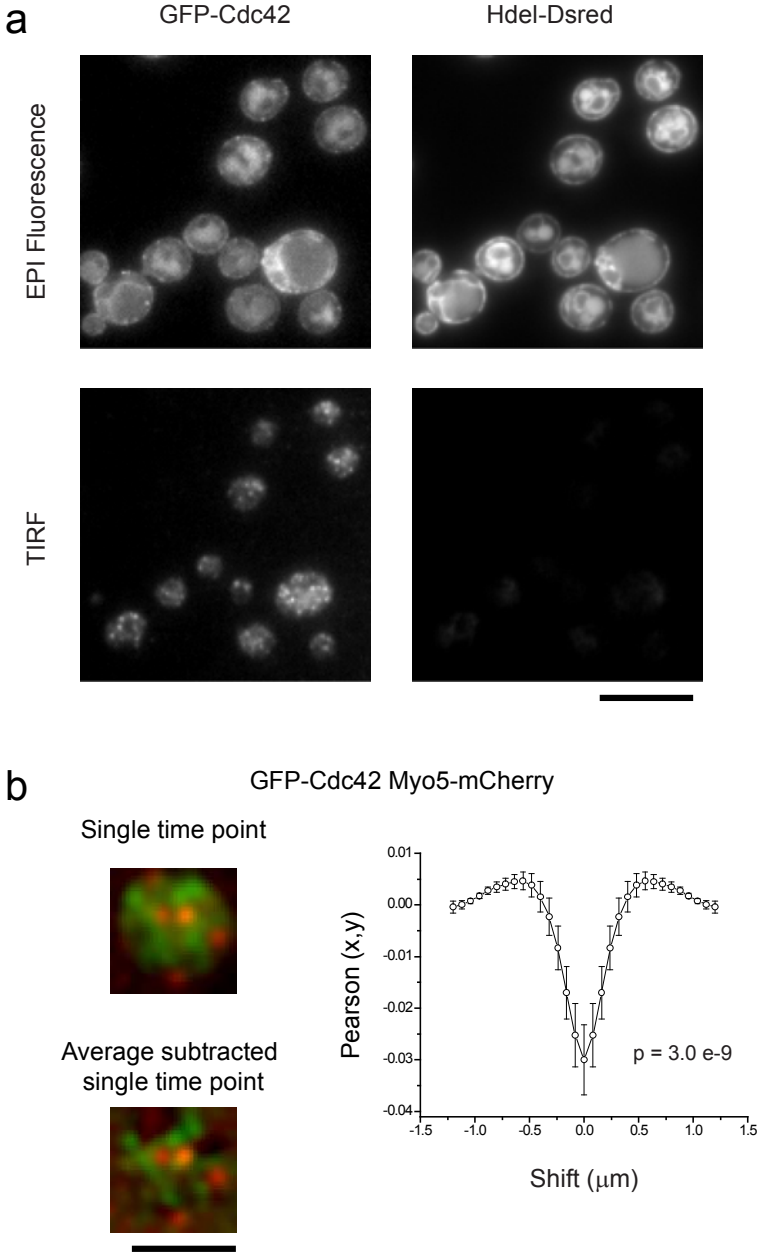

Supplementary Figure S2. TIRF imaging of the Cdc42 microdomains. a. Epi-fluorescence images of GFP-Cdc42 and ER marker Hdel-Dsred, compared to TIRF images. Microdomains of GFP-Cdc42 were clearly visible at a TIRF plane that omitted the cortical ER, demonstrating that the microdomains of Cdc42 are associated with PM, not internal membrane localization. **b**. Two-color analysis of correlation of GFP-Cdc42 and Myo5-mCherry on the PM using TIRF microscopy. A single-time point and average-subtracted time point is shown (See Supplementary Methods). Spatial image cross-correlation was applied to each time point, and averaged for all time points to generate a Pearson correlation plot for each cell. The average for n= 13 cells is shown. Scale bar is 2 μm.

Supplementary Figure S3.

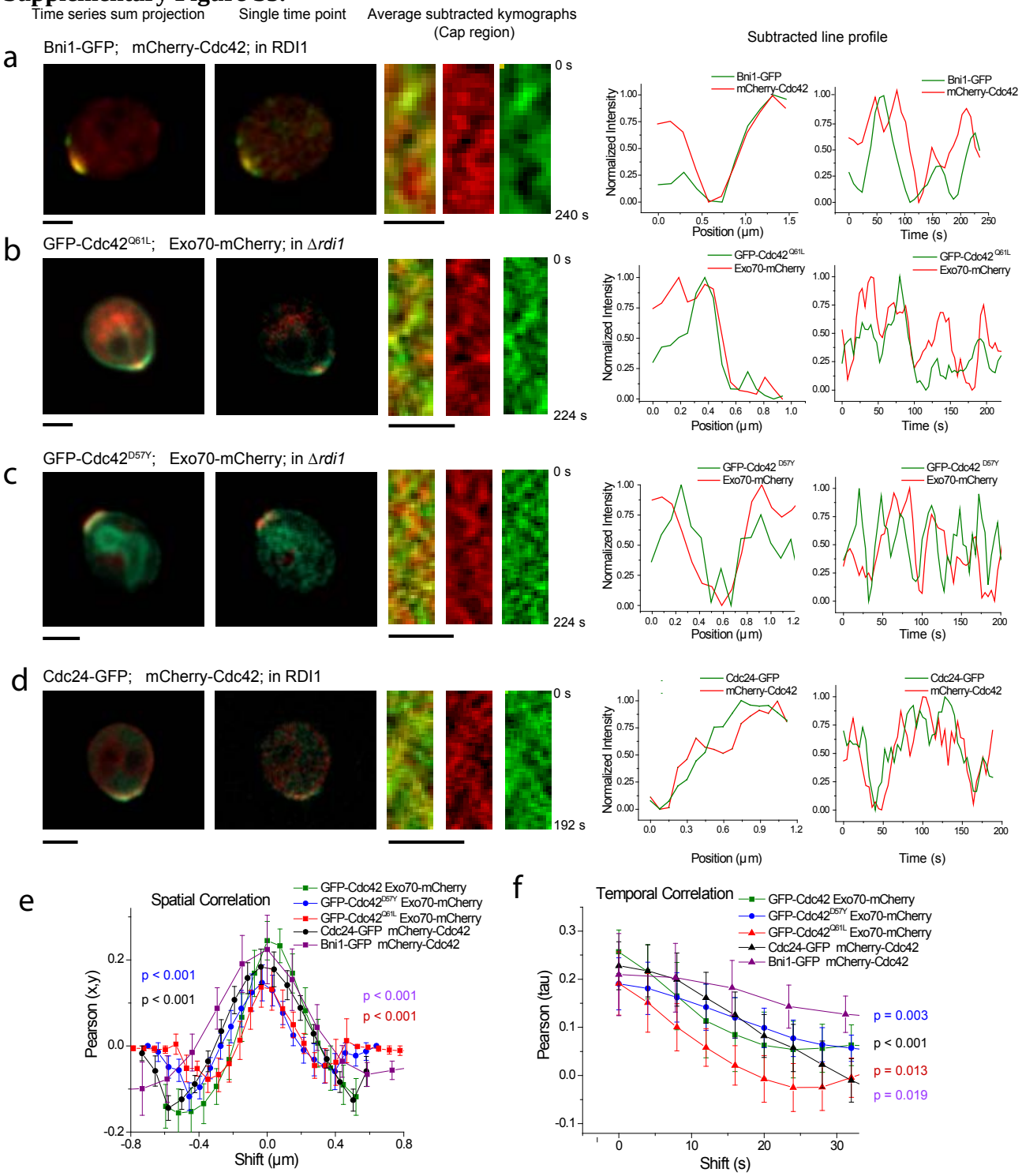

Supplementary Figure S3. Both active and inactive Cdc42 and Cdc42 GEF are enriched in the same microdomains. a-c. Same analysis as shown in main text Figure 1 for Bni1-GFP with mCherry-Cdc42 in the wt background (RDI1) (**a**), Exo70-mChery with GFP-Cdc42^{Q61L} **(b)** and Exo70-mCherry with GFP-Cdc42^{D57Y} in *Δrdi1*, **(c)**, and mCherry-cdc42 with Cdc24-GFP in the RDI1 background **(d)**. The left most column

shows representative time-summed images of the localization of the indicated proteins, while the second column from the left shows an example single time point image. The three columns that follow show sum-subtracted kymographs (merged followed by individual colors) of the polar cap. The second from right plot shows an example average subtracted spatial profile of the cap region, while the right most plots shows example fluorescence traces over time at a single cortical location. Bni1 and Cdc42 were positively correlated in the wt (RDI1) background, similar to the *Δrdi1* background. Like wild-type Cdc42, the GTP (Q61L) and GDP (D57Y) locked Cdc42 mutants were positively correlated with Exo70, suggesting the microdomains do not have a preference for the nucleotide bound state of Cdc42. Positive correlation of Cdc42 and its GEF, Cdc24, was also observed. Scale bars: 2 μm. e,f. Average spatial and temporal correlation.

Supplementary Figure S4.

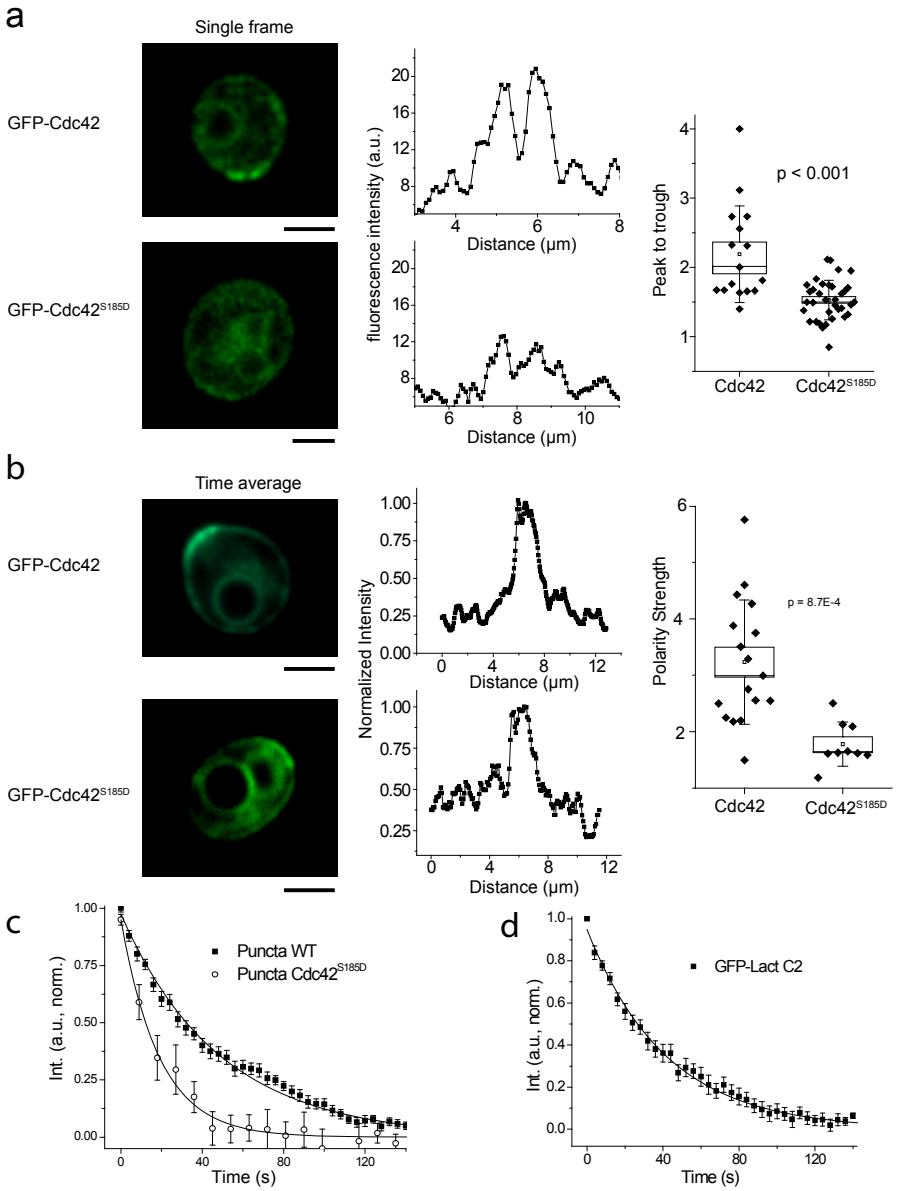

Supplementary Figure S4. Effects of the S185D mutation on Cdc42 diffusion and polarity strength. a. Single frame analysis of peak to trough ratios for Cdc42 and Cdc42^{S185D}. All data came from the *Δrdi1* background. Cells were treated with 50 μM LatA to eliminate recycling and imaged prior to polar cap dissipation. The graphs in the middle show fluorescence traces along the PM of the cells to the left. **b**. Comparison of polarity strength between wild type and mutant (See Supplementary Methods). In each box plot the small box shows the mean, the line median, large box SEM and whiskers SD. **c.** iFRAP decay profiles of Cdc42 and Cdc42^{S185D} puncta in *Δrdi1* cells treated with 50 μM LatA. **d**. Average iFRAP decay profile of GFP-Lact-C2 in *Δrdi1* cells treated with 50 μM LatA. An exponential fit is shown. All scale bars are 2 μm.

Supplementary Figure S5.

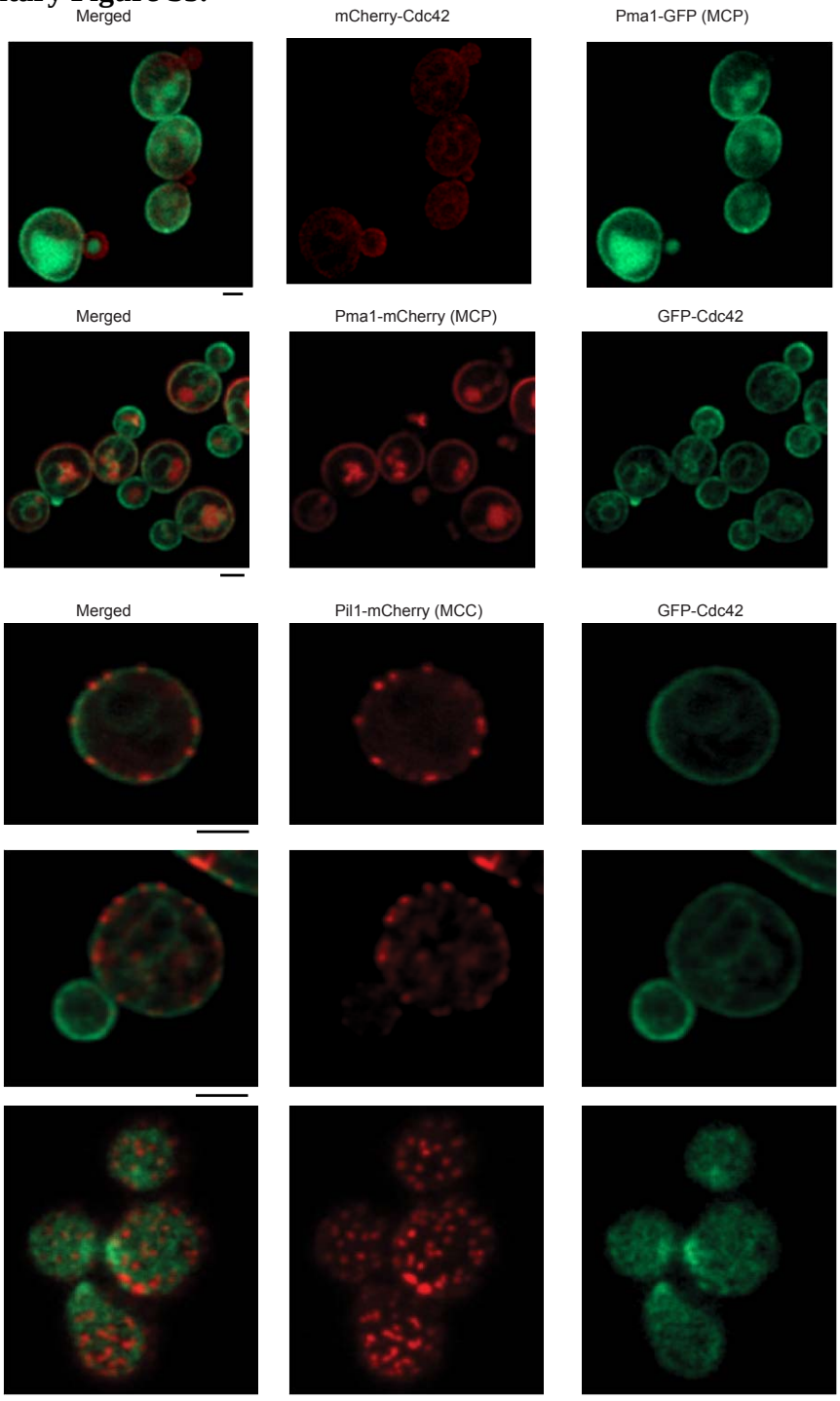

Supplementary Figure S5. Cdc42 puncta do not colocalize with Pma1 or Pil1. Representative images of Pma1-GFP with mCherry-Cdc42, or GFP-Cdc42 with Pma1-mCherry (top) or Pil1-mCherry with GFP-Cdc42 (bottom). For the lowest panel in B, the focus was set to the bottom membrane of the cells. Scale bar is 2 μm.

Supplementary Figure S6.

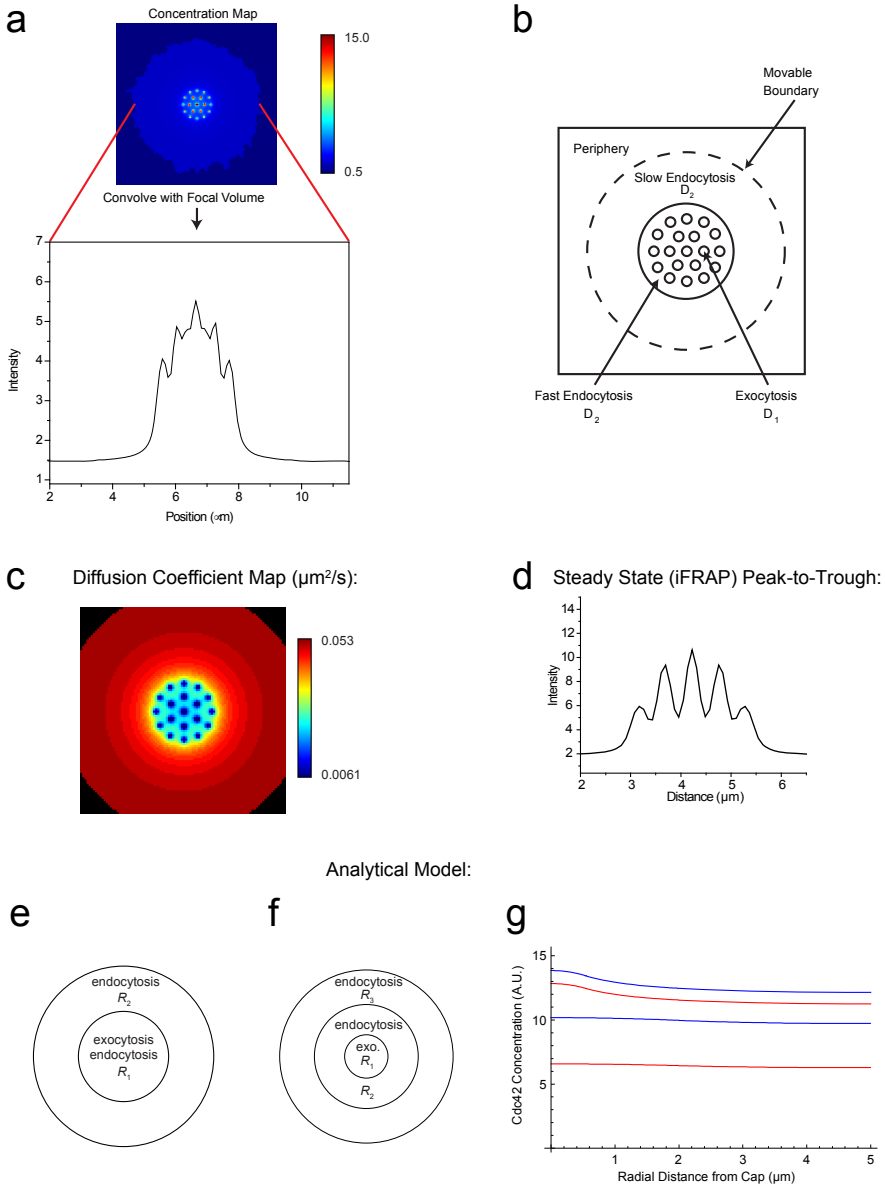

Supplementary Figure S6. Numerical simulation and analytical model of Cdc42 polarity. a. The simulation model 2D profile (top left), 1D profile convolved with the microscope focal volume (bottom left), and (**b**) and an illustration of the compartments used in the simulation **c.** A typical diffusion coefficient heat map used for the iFRAP and membrane traffic models. **d.** The steady-state iFRAP model profile prior to bleaching with diffusion coefficients of 0.053 and 0.0061 $\mu m^2/s$ showing a peak-to-trough ratio approximately matching experimental values. **e-g.** The analytical model geometry and solutions. Model geometry without spatial separation of endocytosis and exocytosis (**e**) and with spatial separation (**f**). (**g**) Radial distribution of Cdc42 protein on the membrane. The blue solid curve corresponds to the case of spatial separation and non-uniform diffusion (as in **d**.) and an exocytic vesicle relative concentration (κ) of 3.4.

The red solid curve corresponds to the above diffusion but with (κ) of 1. The two lower dashed curves are for the case of geometry without the spatial separation of endocytosis and exocytosis with uniform diffusion coefficient D = 0.0013 $\mu m^2/s$ as described for the uniform iFRAP simulations with $\kappa = 3.4$, blue, and $\kappa = 1$, red, Cdc42 accumulation on exocytic vesicles.

Supplementary Figure S7.

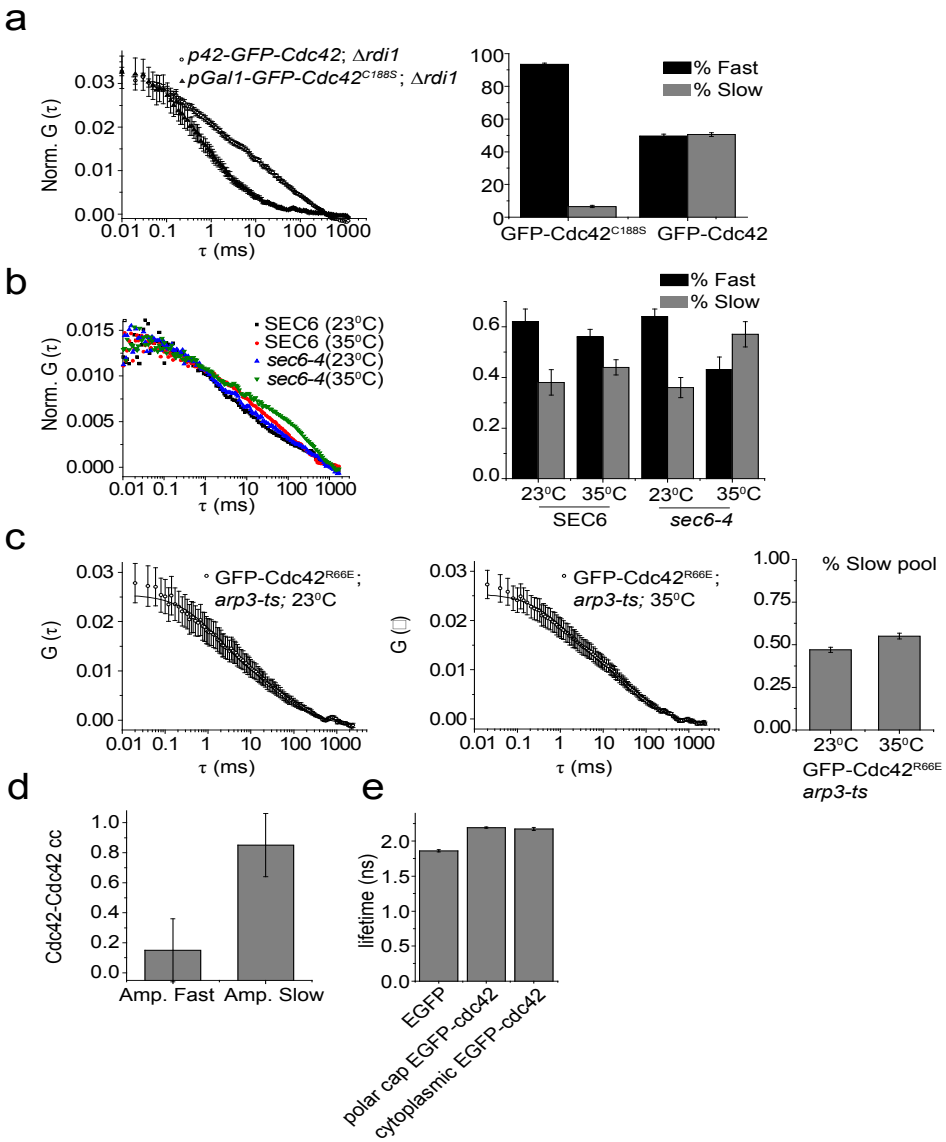

Supplementary Figure S7. Live-cell fluorescence correlation spectroscopy analysis of the slow and fast diffusing pools of Cdc42 in the cytosol. **a**. The presence of the slowly diffusing pool was dependent on Cdc42 prenylation, and was nearly eliminated for the Cdc42^{C188S} non-prenylated mutant[5]. Normalized correlation curves are normalized to the same initial amplitude. **b**. The amplitude of the slowly diffusing pool was dramatically increased in the *sec6-4* mutant at the restrictive temperature. At this temperature, exocytic vesicles accumulate due to their inability to fuse with the plasma membrane[6,7]. **c.** The autocorrelation decay of GFP-Cdc42^{R66E} (defective in Rdi1 binding) in *arp3-2* at the permissive and restrictive temperature was fitted to a two-component model to determine the relative amplitude of the slow pool. The diffusion of the GFP-Cdc42^{R66E} mutant has been shown to recapitulate wild-type Cdc42 in the *Δrdi1* background[8]. The slow pool was not diminished by the reduction in endocytosis at the

restrictive temperature in the ts arp3-2 mutant **d**. Cross-correlation of GFP-Cdc42 and mCherry-Cdc42 was fitted to a two-component model with coefficients of diffusion fixed to the fast and slow transit time for Cdc42. The vast majority of the cross-correlating species of Cdc42 were present in the slowly diffusing pool. **e.** Fluorescence lifetime of cytoplasmic EGFP, EGFP-Cdc42 in the polar cap, and cytoplasmic EGFP-Cdc42. In all bar graphs the error bars represent the standard error in the mean.

Supplementary Figure S8.

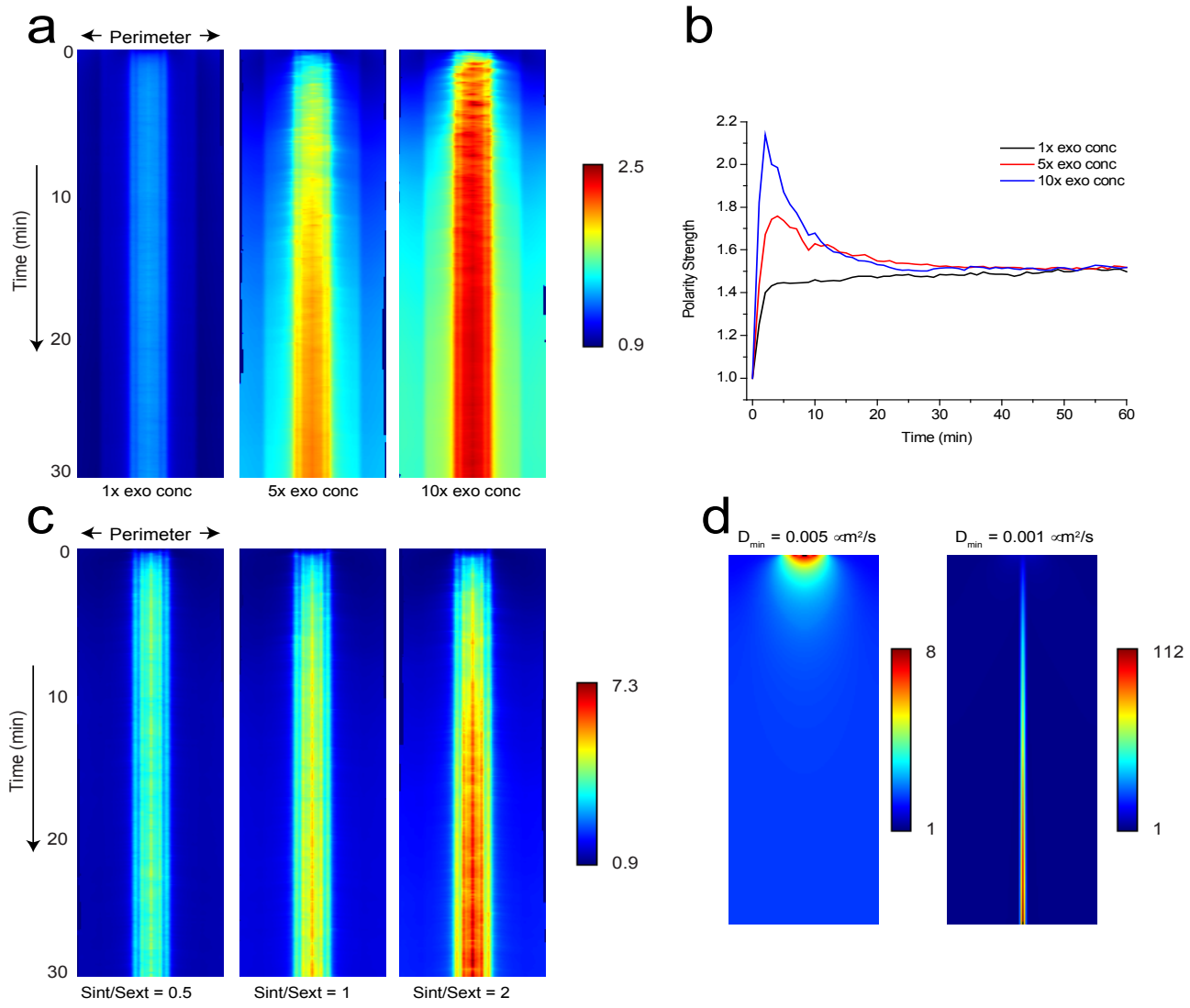

Supplementary Figure S8. **Simulations with varying parameters. a.** Membrane trafficking simulation kymographs performed as in Figure 3G but with D1 = 0.02 $\mu m^2/s$ and D2 = 0.04 $\mu m^2/s$ and different exocytic Cdc42 accumulation ratios as indicated under the kymographs. **b.** Polarity strength plots for the simulations in (**a**). **c.** Effect of changing the relative internal membrane area with other parameters identical to Fig. 3G. **d.** Simulaion kymographs of models for linearly concentration-dependent diffusion with different limiting minimum D values.

Supplementary Table S1.

Table S1. Yeast strains

RLY number	Genotype	Source
2748	*MAT*a; p*BZZ1::GFP:HIS5*	**Slaughter, B**. et. al., *PNAS* 104, 20320 (2007)
4025	*MAT*a; *arp3::HIS5 PDW25 (arp3-2ts :: LEU2) pGAL1-GFP*-myc6-*CDC42*-R*66E CEN URA*	**Winter, D**., et. al., *Curr Biol* 7, 519 (1997)(arp3-2*ts*)
4113	*MAT*a; *sec6-4 pGAL1-GFP-myc6-CDC42 CEN URA*	This study
5046	*MAT*a; *BNI1-GFP::HIS5 pCdc42-mCHERRY-Cdc42* /prs306 *URA3*	This study
6566	*MAT*a; *rdi::LEU2 pGAL1-GFP-myc6-CDC42-S185D CEN URA*	This study
7104	*MAT*a; *rdi::LEU2* pRL369 (p*CDC42-GFP*-myc6-*CDC42* / pRS306 *URA3*)	**Das, A**. et. al., *Nat. Cell. Biol* 14, 304 (2012)
7141	*MAT*a; *rdi1::LEU2 pCDC42-GFP-myc6-CDC42 CEN HIS5 Hygromycin pCdc42-mCHERRY-Cdc42* /pRS306 *URA3*	This study
7142	*MAT*a; *rdi::LEU2* pRL369 (p*CDC42-GFP*-myc6-*CDC42* / pRS306 *URA3*) *MYO5-mCHERRY::HIS5*	This study
7143	*MAT*a; *rdi::LEU2* pRL369 (p*CDC42-GFP*-myc6-*CDC42* / pRS306 *URA3*) *PMA1-mCHERRY::HIS5*	This study
7144	*MAT*a; *rdi::LEU2* pRL369 (p*CDC42-GFP*-myc6-*CDC42* / pRS306 *URA3*) *PIL1-mCHERRY::HIS5*	This study
7146	*MAT*a; *rdi::LEU2 pGAL1-GFP-myc6-CDC42-C188S CEN URA*	This study
7147	*MAT*a; *rdi::LEU2* pRL369 (p*CDC42-GFP*-myc6-*CDC42* / pRS306 *URA3*) *CDC11-mCHERRY::HIS5*	This study
7681	*MAT*a; *rdi1::LEU2 BNI1-GFP::HIS5 pCdc42-mCHERRY-Cdc42* /prs306 *URA3*	This study
7684	*MAT*a; *rdi::LEU2 BNI1-GFP::HIS5 MYO5-mCHERRY::URA3*	This study

7685	*MATa*; rdi::HIS5 *GFP-Lact-C2 CEN URA3 pCdc42-mCherry-Cdc42 /prs305 LEU2*	This study
7737	*MATa*; *rdi::LEU2* pRL369 (p*CDC42-GFP*-myc6-*CDC42* / pRS306 *URA3*) *EXO70-mCHERRY::HIS5*	This study
7764	*MATa*; *rdi::LEU2 pGAL-GFP-myc6-CDC42-D57Y CEN URA3 EXO70-mCherry:HIS5*	This study
7765	*MATa*; *rdi::LEU2 pGAL-GFP-myc6-CDC42-Q61L CEN URA3 EXO70-mCherry:HIS5*	This study
7766	*MATa; pCdc42-mCHERRY-Cdc42* /pRS306 *URA3 PMA1-GFP::HIS5*	This study
7884	*Mata*; *CDC24-GFP::URA3 pCDC42-mCherry-CDC42* /pRS305 *LEU2 Δbem1::KAN*, *pBEM1-BEM1 CEN HIS5*	This study

cells are in the S288C background: his3Δ1;leu2Δ0;met15Δ0;ura3Δ0

Supplementary Methods

Calibrated imaging to determine the Cdc42 level in the polar cap

FCS and calibrated imaging were used to measure Cdc42 concentration at the cap for comparison to that in exocytic vesicles. For unbiased estimation of cortical intensity, it is necessary to remove cytosolic fluorescence. The intensity profile of the cytosol perpendicular to the cortex is the convolution of a step function with the microscope point spread function (PSF). If the PSF is considered to be a Gaussian in the xy plane, this profile is given by an error function. The intensity profile of the cortex, on the other hand, is simply the 1D projection of the PSF. Therefore, the perpendicular intensity profile is given as follows:

$$I(r) = b + I_{edge} \exp\left[\frac{-2(r-r_{edge})^2}{\omega_0^2}\right] + \frac{I_{cyto}}{2}\left(1+\mathrm{erf}\left[\frac{\sqrt{2}(r-r_{edge})}{\omega_0}\right]\right). \qquad \text{(S1)}$$

Here b is the background intensity outside of the cell, I_{edge} is the amplitude of the edge intensity, I_{cyto} is the amplitude of the cytosolic intensity, r_{edge} is the position of the edge, and ω_0 is the PSF "waist" or two times the standard deviation of the PSF.

For experimental determination of the above parameters, photon counting images were acquired with a pixel size of 0.126 μm and an average profile perpendicular to the cortex was obtained over a width of 4 pixels using a custom ImageJ plugin. This profile was then fit to the above function using non-linear least squares also with a custom ImageJ plugin to obtain the parameters of interest, namely I_{edge}. The concentration on the membrane is related to its intensity amplitude (I_{edge}) as follows:

$$I_{edge} = \varepsilon_{GFP} C A_{PSF} \tag{S2}$$

Here ε_{GFP} is the molecular brightness of GFP at the center of the PSF in units of counts per pixel dwell time as defined above. C is the membrane concentration and A is the area of the PSF on the membrane. The GFP molecular brightness can be determined from an equivalent image of yeast expressing 1x GFP as well as FCS measurements on that same cell as follows:

$$\varepsilon_{GFP} = \frac{I \cdot G(0)}{\gamma}. \tag{S3}$$

Here I is the average image intensity, not the intensity from the FCS measurement and both FCS and imaging are done with the same pinhole settings. The area of the PSF on the membrane was calculated as 0.6 μm^2 from an xz cross section of a 3D image of a 100 nm fluorescent bead taken with the same pinhole settings as the confocal imaging. The gamma factor was calculated from the same measurement using the following formula (*3*):

$$\gamma = \frac{\int PSF^2(\vec{r})d\vec{r}}{\int PSF(\vec{r})d\vec{r}}. \tag{S4}$$

Calculation of polarity strength

To calculate polarity strength, a time average of GFP-Cdc42 fluorescence was obtained and the perimeter profile was fitted to a Gaussian distribution. The polarity strength (Fig. 4F, Fig. S4b) was defined as the peak value compared to the baseline.

Total Internal Reflection Fluorescence microscopy

TIRF imaging was carried out using a Nikon TE2000 inverted microscope (Nikon Instruments , Melville, NY) equipped with a T-Fl-TIRF 2 Illuminator, a CFI APO 60X Oil TIRF NA 1.49 objective, a Chroma dichroic filter Z488/561x (Bellows Falls, VT), and a Photometrics CoolSnap HQ^2 camera (Tucson, AZ). Laser excitation sources for TIRF were Coherent Sapphire 488-50 and Sapphire 561-50 (Santa Clara, CA) and the Epi-fluorescence excitation source was an XCite Series 120 lamp (Lumen Dynamics Group, Mississaugua, Ontario). For GFP-Cdc42 and Myo5-mCherry TIRF experiments, time series were acquired at 3s/timepoint for 100 to 200 timepoints per movie. The GFP-Cdc42 was imaged with Chroma emission filter ET525/50m and exposure time of 200ms. DsRed was imaged with a Chroma emission filter ET600/50m and exposure time 1s.

For GFP-Cdc42, Hdel-DsRed images, GFP exposure was set to 700ms and DsRed was imaged with Chroma emission filter ZET488/561m and exposure 200ms. Image drift was corrected using a custom image alignment plugin in ImageJ, and averages were generated of six sequential time points (over a 50 second period) in the series, with 2 x 2 pixel spatially binning. Epi-fluorescence images are single images binned 2 x 2 and were taken with Chroma filter sets FITC HYQ (460-500, 505, 510-560) for GFP and TRITC HYQ (530-560, 570, 590-650) for mCherry, respectively, with exposure 700ms. Images were corrected for differences in exposure times.

For two-color TIRF movies of GFP-Cdc42 and Myo5-mCherry, the same filter sets were used as described above. Images for red and green were taken at 3 second intervals. Prior to spatial cross-correlation, the average green and red images were subtracted from each time point. Spatial image cross-correlation[55] was applied to each

image (a simple two dimensional extension of our earlier 1D analysis), and the average for all frames was generated.

Fluorescence lifetime imaging

Fluorescence lifetime imaging was performed essentially as described in Shivaraju et al. 2012 [56]. Briefly, excitation was accomplished with two photon excitation at 920 nm and emission was collected with the Carl Zeiss Confocor3 module with a Becker and Hickl SPC-830 FLIM acquisition board (Berlin, Germany). Fluorescence decay profiles were created from cytosolic and polar cap regions. These were then fit to single exponential decays with iterative reconvolution using an instrument response function generated from SHG of urea crystals. This was repeated for many cells to obtain average lifetimes and SEM values. The lifetime of GFP was 1.86 ns (SEM = 0.02). The lifetimes of cap and cytosolic GFP-cdc42 were 2.19 (SEM = 0.01) and 2.17 (SEM = 0.02) ns, respectively.

Simulations of polarity establishment

Simulations were written with custom Java code and kymographs were generated using ImageJ. The simulation was performed in a similar way to Layton et al.[10] with a few changes to simplify the coding of the model and allow for non-uniform diffusion. Briefly, the model consists of a two-dimensional array of intensities larger than the size of the circular membrane as well as a matching two-dimensional Boolean mask denoting the membrane shape and a central circular window of exocytosis that also contains enhanced endocytosis. The model also included an internal membrane that is considered

well mixed. Addition of more internal membrane area did not affect simulations that include non-uniform diffusion, as these already achieve prolonged polarity (not shown), but did prolong initial cap formation in simulations in the case of uniform diffusion, where depletion of the internal pool eventually leads to cap dissipation (Fig. S8c). As a variation on the Layton et al. method, we chose to physically expand the membrane in response to exocytosis and contract it in response to endocytosis rather than re-interpolating the membrane to maintain the grid size. The expansion and contraction was made isotropic by randomly rotating the entire membrane before a horizontal insertion or removal and randomly rotating back after insertion or removal. Membrane external to the insertion or removal site was shifted outward or inward to accommodate new material so as to avoid shifting of the cortical cap material. The region outside of the boundary was filled with the average of the boundary at each time step to ensure that interpolation associated with rotations did not lead to loss of protein. Despite these precautions, large diffusion coefficients outside the cap combined with the Gaussian convolution simulation method described below inevitably lead to a small amount of protein loss. Therefore, we added protein uniformly to the cap at each time stamp to maintain the total protein at a constant level. As with the Layton et al. paper, the pixel size was set to 0.088 μm with a surface area equivalent to the surface area of a 50 μm diameter endocytic sphere. In this way, a single pixel is removed during endocytosis and four pixels are added during exocytosis.

Diffusion in our simulation was accomplished with a Gaussian convolution mechanism reminiscent of single particle tracking simulations[57]. We cannot use the standard finite differences approaches as they do not allow for non-uniform diffusion

coefficients. For Brownian motion, the probability of a particle moving distance *d* in two dimensions with a shift in time Δt is given as follows:

$$P(d,\Delta t) = \exp\left[-d^2 \Big/ 4D(\vec{r})\Delta t\right] \Big/ 2\pi\sigma^2 . \quad \text{(S5)}$$

Simply stated, this is a Gaussian distribution with standard deviation $\sqrt{2D(\vec{r})\Delta t}$. Note that *D* is written as a spatially dependent variable. Given this simple model, the update rule for each pixel in our simulation at each frame is the sum of the neighboring probability distributions multiplied by their center intensities as follows:

$$I(\vec{r},t+T) = \sum_{\vec{\rho}} I(\vec{\rho},t)P(\left|\vec{\rho}-\vec{r}\right|,T) . \quad \text{(S6)}$$

As is shown by Fig. 3B and 3C, these modifications do not significantly affect the results.

With these modifications, we extended the Layton et al. model to include a diffusion trap by spatially restricting exocytosis to 19 3x3 pixel regions coinciding with the valleys of the diffusion coefficient map (Fig. S6B and iFRAP simulation methods). Endocytosis was eliminated from these regions (Fig. S6B). Kymographs were generated by convolving the distribution with an asymmetric Gaussian simulating a vertical membrane intersecting a confocal image. The radial waist of the Gaussian was set to 0.2 μm and the axial waist was set to 0.8 μm as expected for a 1.2 NA water objective such as the one used for the experiments in this article. Polarity strengths were determined by the max/min ratio of the kymograph. Polarity durations were measured as the amount of time that the polarity strength was above 1.3, the maximum polarity strength achieved under uniform diffusion and 10x exocytic concentration (see Fig.3c and j).

Concentration Dependent Diffusion

One possible model for generating nonuniform diffusion is one in which diffusion is concentration dependent. We modeled this scenario in the following way: The simulation was started with an initial protein distribution equivalent to the steady state distribution observed before bleaching in the iFRAP simulations. Protein densities were mapped to diffusion coefficients in an inverse linear fashion with lowest densities corresponding to a maximum diffusion coefficient of 0.05 $\mu m^2/s$ and highest densities corresponding to 80% of the chosen limiting minimum diffusion coefficient. The diffusion coefficients were mapped to 40 linearly distributed values to allow for lookup tables as described in the iFRAP simulation methods. Diffusion simulations were performed as for the iFRAP simulation, but at each time step, the diffusion coefficient profile was remapped to the current protein densities. In regions where densities mapped to diffusion coefficients below the minimum and above the maximum value the diffusion coefficients were set to the minimum and maximum values, respectively. Minimum D values reported are 0.005 and 0.001 $\mu m^2/s$ (Fig. S8d).

Analytical model

Continuous model: no spatial separation

Consider a model of Cdc42 protein dynamics on the surface of a polarized yeast cell. The standard model considers the case of a single transport window on the cell membrane surface. The dynamics of the protein concentration is described by the following equations

$$\frac{\partial f_1}{\partial t} = D_1 \Delta f_1 - m f_1 + h F_{int}, \quad 0 \le r \le d, \tag{S7}$$

$$\frac{\partial f_2}{\partial t} = D_2 \Delta f_2 - n f_2, \, d \le r \le L, \tag{S8}$$

where in the cap area represented by a circle R_1 with the radius d both endocytosis and exocytosis take place, while in the remaining part of the external membrane R_2 with the outer radius L slower endocytosis is observed (the geometry of this model is shown in Figure S6e). Here the diffusion coefficients $D_i, i = 1,2,$ correspond to the regions R_i. A quantity F_{int} denotes total protein amount on the internal membrane, it can be found from the total protein conservation condition

$$F_{tot} = F_{int} + \int_{R_1} f_1 dr + \int_{R_2} f_2 dr = const. \tag{S9}$$

In (S7-S8) h denotes the exocytosis rate, while m and n are the rates of endocytosis. The model assumes unifom diffusion over the external membrane, so that $D_1 = D_2 = D$.

The model geometry implies axial symmetry of the solution, so that the Laplacian operator Δ in the polar coordinates $\{r, \phi\}$ reduces to

$$\Delta f = \frac{1}{r} \frac{\partial}{\partial r} \left(r \frac{\partial f}{\partial r} \right) \tag{S10}$$

The equations (S7-S8) are subject to no-flux boundary conditions at $r = 0, L$:

$$f_1'(0) = 0, \quad f_2'(L) = 0. \tag{S11}$$

The solutions also should be matched at the inner boundary at $r = d$

$$f_1(d) = f_2(d), \, f_1'(d) = f_2'(d), \tag{S12}$$

with the additional condition $f_1(0) = G$ where the value G at the origin is undetermined yet.

In steady state the problem (S7-S8) reduces to

$$D\Delta f_1 = mf_1 - hF_{int}, \tag{S13}$$

$$D\Delta f_2 = nf_2. \tag{S14}$$

The general solution of this system reads

$$f_1 = \frac{hF_{int}}{m} + C_1 I_0(Mr), f_2 = C_2 I_0(Nr) + C_3 K_0(Nr), \tag{S15}$$

where I_0 and K_0 denotes modified Bessel function of first and second kind respectively. The parameters M and N are defined through

$$M^2 = m/D, \quad N^2 = n/D. \tag{S16}$$

The three coefficients $C_i, i = 1,2,3,$ are determined from the boundary conditions (S11,S12); the explicit expressions are cumbersome and are not presented here. Using the solutions (S15) in (S9) we obtain the steady state value of the internal membrane protein amount F_{int}.

Continuous model: spatial separation

The experimental data hints that the spatial structure of the external membrane is more complex. Below we introduce a model in which the cap area consists of a central circular area (region R_1) of the radius r_0 where exocytosis only takes place and the ring around it (region R_2 with external radius d) that contains the actin patches responsible for endocytosis. The external circular area (region R_3 with external radius L) outside the cap is characterized by endocytosis with slower internalization rate than that of in the cap region (see Figure S6f).

The external membrane equations are written in the form

$$\frac{\partial f_1}{\partial t} = D_1 \Delta f_1 + hF_{int}, \quad 0 \le r \le r_0, \tag{S17}$$

$$\frac{\partial f_2}{\partial t} = D_2 \Delta f_2 - mf_2, \, r_0 \le r \le d, \tag{S18}$$

$$\frac{\partial f_3}{\partial t} = D_3 \Delta f_3 - nf_3, \; d \le r \le L, \tag{S19}$$

where the diffusion coefficients $D_i, i = 1,2,3,$ correspond to the regions R_i. The total protein amount F_{int} on the internal membrane, is found from the total protein conservation condition

$$F_{tot} = F_{int} + \int_{R_1} f_1 dr + \int_{R_2} f_2 dr + \int_{R_3} f_3 dr = const. \tag{S20}$$

The equations (S17-S20) are subject to no-flux boundary conditions at $r = 0, L$:

$$f_1'(0) = 0, \quad f_3'(L) = 0. \tag{S21}$$

The solutions also should be matched at both inner boundaries at $r = r_0$ and $r = d$

$$f_1(r_0) = f_2(r_0), \, f_1'(r_0) = f_2'(r_0), \; f_2(d) = f_3(d), \; f_2'(d) = f_3'(d), \tag{S22}$$

with the additional condition $f_1(0) = G$ where the value G at the origin is undetermined yet.

The measurements show that the diffusion is slower inside the exocytic central region R_1 as shown in Figure S6f, so that we approximate the diffusion coefficients as follows

$$D_1 = D(1 - A), \; D_2 = D_3 = D. \tag{S23}$$

In steady state the problem (S17-S19) reduces to

$$D_1 \Delta f_1 = -hF_{int}, \tag{S24}$$

$$D\Delta f_2 = mf_2, \tag{S25}$$

$$D\Delta f_3 = nf_3. \qquad \text{(S26)}$$

The general solution of this system reads

$$f_1 = \frac{G - hF_{int}r^2}{4D_1},\ f_2 = C_1 I_0(Mr) + C_2 K_0(Mr),\ \ f_3 = C_3 I_0(Nr) + C_4 K_0(Nr). \qquad \text{(S27)}$$

The four coefficients C_i and the value of G are determined from the boundary conditions (S21,S22); the explicit expressions are very cumbersome and are not presented here. Using these expressions in condition (S20) leads to determination of F_{int} which explicit expression is omitted too.

Quasidiscrete model

The model (S17-S19) can be adopted to describe vesicle-based mechanism of protein transport. We start consideration of the discrete vesicle based model by introducing the notation. The size of the internal cytosolic membrane is S_{int}, while the external cellular membrane has area $S_{ext} = \pi L^2$. We assume that the exchange of the vesicles between the membranes does not change their areas. The external membrane is made of three regions with the areas $S_1 = \pi r_0^2$, $S_2 = \pi(d^2 - r_0^2)$ and $S_3 = \pi(L^2 - d^2)$. The exocytosis rate (the off rate of the internal membrane) is k_{int}, and the surface area of exocytic and endocytic vesicles is A_{ex} and A_{en}, respectively. The endocytosis rates (the off rates of the external membrane) k_2 and k_3 are considered below. The conservation of the membranes surface area leads to the condition

$$(k_2 + k_3)A_{en} = k_{ext}A_{en} = k_{int}A_{ex} = K. \qquad \text{(S28)}$$

In the region R_1 the dynamics of the external membrane Cdc42 density f_1 is governed by the protein diffusion and exocytosis from the internal membrane, so that it is described by the equation

$$\frac{\partial f_1}{\partial t} = D_1 \Delta f_1 + \frac{k_{int} A_{ex} \kappa \rho_{int}}{S_1}, \quad 0 \le r \le r_0, \tag{S29}$$

where D_1 is the local diffusion coefficient, ρ_{int} denotes the uniform internal membrane Cdc42 concentration and κ is the accumulation coefficient, i.e., we assume that the exocytic vesicle protein concentration is κ times larger than of internal membrane. The source term is proportional to the number of exocytic vesicles per unit of time k_{int}, their surface area A_{ex} and the concentration of the protein on each vesicle $\kappa\rho_{int}$. The vesicles are uniformly spread inside the region R_1, so that the source term is inversely proportional to the region surface area S_1.

In the regions R_2, R_3 the protein is removed from the external membrane, so that we have

$$\frac{\partial f_2}{\partial t} = D \Delta f_2 - \frac{k_2 A_{en} f_2}{S_2}, \quad r_0 \le r \le d, \tag{S30}$$

$$\frac{\partial f_3}{\partial t} = D \Delta f_3 - \frac{k_3 A_{en} f_3}{S_3}, \quad d \le r \le L, \tag{S31}$$

where $D = D_2$ is the local diffusion coefficient.

Parameters Estimate

Comparing the equations (S29-S31) with (S17-S19) we find for the protein endocytic rates m and n

$$m = \frac{k_2 A_{en}}{S_2},\ n = \frac{k_3 A_{en}}{S_3}, \tag{S32}$$

so that their ratio is computed as

$$R = \frac{m}{n} = \frac{S_3 k_2}{S_2 k_3}. \tag{S33}$$

The protein exocytic rate reads

$$h = \frac{k_{int} \kappa A_{ex}}{S_{int} S_1}. \tag{S34}$$

From (S32) using the ratio R definition we find

$$k_2 = \frac{k_{ext}}{1 + S_3/(RS_2)},\quad k_3 = \frac{k_{ext}}{1 + RS_2/S_3}. \tag{S35}$$

Using the relation $D_1 = D(1 - A),$ denote the value of the diffusion averaged over whole membrane as D_{av}, which can be computed as

$$D_{av} = \frac{2}{L^2}\left(\int_0^{r_0} D_1 r dr + \int_{r_0}^{L} D r dr\right) = \frac{D}{L^2}(L^2 - A r_0^2). \tag{S36}$$

This relation can be used to compute the value of parameter D. The region sizes were estimated as

$$r_0 = 0.55\ \mu m, d = 2.0\ \mu m, L = 5\ \mu m. \tag{S37}$$

The area of the internal membrane S_{int} was made equal to total area of the external membrane πL^2. The parameters values were selected as

$$R = 3,\ D_{av} = 0.013\ \mu m^2/s,\ A = 0.6,\ k_{ext} = 1.67\ 1/s,\ \kappa = 3.4,\ A_{en} = 0.0077\ \mu m^2,\ F_{tot} = 1000. \tag{S38}$$

The distribution of protein concentration on the external membrane computed with the above parameters is presented in Figure S6g.

Supplementary Figure Legends

Supplementary Figure S1. Non-average subtracted data corresponding to the data shown in Figure 1. A time series-sum projection (left), along with raw kymographs (merged followed by individual channels) of GFP-Cdc42 with Myo5-mCherry (**a**), Bni1-GFP with Myo5-mCherry (**b**), Bni1-GFP with mCherry-Cdc42 (**c**), GFP-Cdc42 with Exo70-mCherry (**d**), and mCherry-Cdc42 with GFP-Lact-C2 (**e**). Scale bars: 2 μm. The plots on the right compare show normalized average line profiles (averaged over time for each kymograph) and a normalized average-subtracted single line profile for the green and red-labeled proteins. Note that on a cell perimeter-wide, average scale, there will be overlap of any pair of polarized proteins. However, line profiles generated from single images (without average subtraction (right column), or with average subtraction, show non-smooth distributions. (See also Figure 1 and Methods in Supplementary Information).

Supplementary Figure S2. TIRF imaging of the Cdc42 microdomains. a. Epi-fluorescence images of GFP-Cdc42 and ER marker Hdel-Dsred, compared to TIRF images. Microdomains of GFP-Cdc42 were clearly visible at a TIRF plane that omitted the cortical ER, demonstrating that the microdomains of Cdc42 are associated with PM, not internal membrane localization. **b**. Two-color analysis of correlation of GFP-Cdc42 and Myo5-mCherry on the PM using TIRF microscopy. A single-time point and average-subtracted time point is shown (See Supplementary Methods). Spatial image

cross-correlation was applied to each time point, and averaged for all time points to generate a Pearson correlation plot for each cell. The average for n= 13 cells is shown.

Supplementary Figure S3. Both active and inactive Cdc42 and Cdc42 GEF are enriched in the same microdomains. a-c. Same analysis as shown in main text Figure 1 for Bni1-GFP with mCherry-Cdc42 in the wt background (RDI1) (**a**), Exo70-mChery with GFP-Cdc42^{Q61L} **(b)** and Exo70-mChery with GFP-Cdc42^{D57Y} in *Δrdi1*, **(c)**, and mCherry-cdc42 with Cdc24-GFP in the RDI1 background **(d)**. The left most column shows representative time-summed images of the localization of the indicated proteins, while the second column from the left shows an example single time point image. The three columns that follow show sum-subtracted kymographs (merged followed by individual colors) of the polar cap. The second from right plot shows an example average subtracted spatial profile of the cap region, while the right most plots shows example fluorescence traces over time at a single cortical location. Bni1 and Cdc42 were positively correlated in the wt (RDI1) background, similar to the *Δrdi1* background. Like wild-type Cdc42, the GTP (Q61L) and GDP (D57Y) locked Cdc42 mutants were positively correlated with Exo70, suggesting the microdomains do not have a preference for the nucleotide bound state of Cdc42. Positive correlation of Cdc42 and its GEF, Cdc24, was also observed. Scale bars: 2 μm. e,f. Average spatial and temporal correlation.

Supplementary Figure S4. Effects of the S185D mutation on Cdc42 diffusion and polarity strength. a. Single frame analysis of peak to trough ratios for Cdc42 and Cdc42^{S185D}. All data came from the *Δrdi1* background. Cells were treated with 50 μM LatA to eliminate recycling and imaged prior to polar cap dissipation. The graphs in the middle show fluorescence traces along the PM of the cells to the left. **b**. Comparison of polarity strength between wild type and mutant (See Supplementary Methods). In each box plot the small box shows the mean, the line median, large box SEM and whiskers SD. **c.** iFRAP decay profiles of Cdc42 and Cdc42^{S185D} puncta in *Δrdi1* cells treated with 50 μM LatA. **d**. Average iFRAP decay profile of GFP-Lact-C2 in *Δrdi1* cells treated with 50 μM LatA. An exponential fit is shown. All scale bars are 2 μm.

Supplementary Figure S5. Cdc42 puncta do not colocalize with Pma1 or Pil1. Representative images of Pma1-GFP with mCherry-Cdc42, or GFP-Cdc42 with Pma1-mCherry (top) or Pil1-mCherry with GFP-Cdc42 (bottom). For the lowest panel in B, the focus was set to the bottom membrane of the cells. Scale bar is 2 μm.

Supplementary Figure S6. Numerical simulation and analytical model of Cdc42 polarity. a. The simulation model 2D profile (top left), 1D profile convolved with the microscope focal volume (bottom left), and (**b**) and an illustration of the compartments used in the simulation **c.** A typical diffusion coefficient heat map used for the iFRAP and membrane traffic models. **d.** The steady-state iFRAP model profile prior to bleaching with diffusion coefficients of 0.053 and 0.0061 μm^2/s showing a peak-to-trough ratio approximately matching experimental values. **e-g.** The analytical model

geometry and solutions. Model geometry without spatial separation of endocytosis and exocytosis (**e**) and with spatial separation (**f**). (**g**) Radial distribution of Cdc42 protein on the membrane. The blue solid curve corresponds to the case of spatial separation and non-uniform diffusion (as in **d**.) and an exocytic vesicle relative concentration (κ) of 3.4. The red solid curve corresponds to the above diffusion but with (κ) of 1. The two lower dashed curves are for the case of geometry without the spatial separation of endocytosis and exocytosis with uniform diffusion coefficient D = 0.0013 $\mu m^2/s$ as described for the uniform iFRAP simulations with $\kappa = 3.4$, blue, and $\kappa = 1$, red, Cdc42 accumulation on exocytic vesicles.

Supplementary Figure S7. **Live-cell fluorescence correlation spectroscopy analysis of the slow and fast diffusing pools of Cdc42 in the cytosol. a**. The presence of the slowly diffusing pool was dependent on Cdc42 prenylation, and was nearly eliminated for the $Cdc42^{C188S}$ non-prenylated mutant[25]. **b**. The amplitude of the slowly diffusing pool was dramatically increased in the *sec6-4* mutant at the restrictive temperature. At this temperature, exocytic vesicles accumulate due to their inability to fuse with the plasma membrane[26,27]. **c.** The autocorrelation decay of GFP-$Cdc42^{R66E}$ (defective in Rdi1 binding) in *arp3-2* at the permissive and restrictive temperature was fitted to a two-component model to determine the relative amplitude of the slow pool. The diffusion of the GFP-$Cdc42^{R66E}$ mutant has been shown to recapitulate wild-type Cdc42 in the *Δrdi1* background[21]. The slow pool was not diminished by the reduction in endocytosis at the restrictive temperature in the ts arp3-2 mutant **d**. Cross-correlation of GFP-Cdc42 and mCherry-Cdc42 was fitted to a two-component model with coefficients of diffusion fixed

to the fast and slow transit time for Cdc42. The vast majority of the cross-correlating species of Cdc42 were present in the slowly diffusing pool. In all bar graphs, the error bars represent the SEM. e. Fluorescence lifetime of cytoplasmic EGFP, EGFP-Cdc42 in the polar cap, and cytoplasmic EGFP-Cdc42. Error bars represent the standard error in the mean.

Supplementary Figure S8. **Simulations with varying parameters. a.** Membrane trafficking simulation kymographs performed as in Figure 3G but with D1 = 0.02 $\mu m^2/s$ and D2 = 0.04 $\mu m^2/s$ and different exocytic Cdc42 accumulation ratios as indicated under the kymographs. **b.** Polarity strength plots for the simulations in (**a**). **c.** Effect of changing the relative internal membrane area with other parameters identical to Fig. 3G. **d.** Simulaion kymographs of models for linearly concentration-dependent diffusion with different limiting minimum D values.

Supplementary References:

55. Costantino, S., Comeau, J.W., Kolin, D.L. & Wiseman, P.W. Accuracy and dynamic range of spatial image correlation and cross-correlation spectroscopy. *Biophys J* **89**, 1251-1260 (2005).
56. Shivaraju, M. et al. Cell-cycle-coupled structural oscillation of centromeric nucleosomes in yeast. *Cell* **150**, 304-316 (2012).
57. Dietrich, C., Yang, B., Fujiwara, T., Kusumi, A. & Jacobson, K. Relationship of lipid rafts to transient confinement zones detected by single particle tracking. *Biophys J* **82**, 274-284 (2002).